Article:

Generating quantum correlated photon pairs in a hybrid silicon–BTO platform

D. Marchant ✉ ⓘ ; I. Faruque ⓘ ; J. Barreto ⓘ

Check for updates

View Online   Export Citation

Articles You May Be Interested In

Giant anomalous self-steepening and temporal soliton compression in silicon photonic crystal waveguides

APL Photonics (August 2021)

ITO-based electro-absorption modulator for photonic neural activation function

APL Mater. (August 2019)

Selective photothermal self-excitation of mechanical modes of a micro-cantilever for force microscopy

Appl. Phys. Lett. (October 2011)

Generating quantum correlated photon pairs in a hybrid silicon–BTO platform

D. Marchant,[1,2,a]   I. Faruque,[1]   and J. Barreto[1]

AFFILIATIONS

[1] Quantum Engineering Technology Labs, University of Bristol, NSQI building, Tyndall Avenue, Bristol BS8 1FD, England
[2] Quantum Engineering Centre for Doctoral Training, University of Bristol, NSQI building, Tyndall Avenue, Bristol BS8 1FD, England

[a] Author to whom correspondence should be addressed: d.marchant@bristol.ac.uk

ABSTRACT

Here, we show photon pair generation from ring resonator and waveguide structures in a hybrid silicon–BTO on an insulator platform with a pulsed pump. Our analysis of single photon and coincidence generation rates show that spontaneous four-wave mixing is comparable to that expected from SOI devices with similar characteristics and find γ_{eff} of (14.7 ± 1.3) and (2.0 ± 0.3) MHz/mW^2 for ring resonator and waveguide structures, respectively.

I. INTRODUCTION

Photon pair sources are a key building block for linear optical quantum computing[1,2] and quantum communication.[3,4] On-chip quantum information processing requires the capability of producing photon pairs with high brightness and high speed modulation. A hybrid Si–BaTiO$_3$ (Si-BTO) platform was shown by Eltes *et al.*[5] to fulfill the latter, and here, we show that it also fulfills the former requirement. This is in addition to cryogenic compatibility,[6] a requirement for full integration of integrated photonic circuits with SNSPDs, complementary metal-oxide-semiconductor (CMOS) compatibility,[7] and low loss.[8]

Integrated photon pair sources can be realized using spontaneous parametric down conversion (SPDC), a $\chi^{(2)}$ process, or SFWM, a $\chi^{(3)}$ process.[9] In these two processes, one (in SPDC) or two (in SFWM) photons from the pump source are annihilated and two photons, a signal photon and idler photon, are generated at energy matched frequencies detuned from the pump. The frequency detuning of the generated photons allows them to be spectrally filtered from the pump photons. Although the $\chi^{(2)}$ coefficient of a material is typically an order of magnitude larger,[10] we have more freedom in exploiting the $\chi^{(3)}$ coefficient as it does not require a wide transparency window. In this article, we focus on the photon generation properties from SFWM.

It is often desirable to be able to tune the effective refractive index of the waveguide for integrated photonics applications. For example, multiplexing schemes can be realized using Mach–Zhender interferemoters (MZIs) to route photons to different outputs by applying a phase shift to one arm. In materials that do not have a significant $\chi^{(2)}$ response, such as Si, this leaves either thermo-optic (TO) modulation,[11] plasma dispersion (PD) modulation,[12] or electro-optic (EO) modulation via the $\chi^{(3)}$ Kerr effect.[13] The TO effect is limited to kHz speeds and its magnitude is reduced at cryogenic temperatures.[14] PD modulators also have poor cryogenic compatibility due to carrier freeze out at low temperatures. While Kerr effect EO modulators are cryogenically compatible, the tuning efficiency is poor, leading to large device footprints. Another option is to integrate Si waveguides with a material capable of EO modulation via $\chi^{(2)}$ Pockels effect, which has been shown to achieve high speed modulation at cryogenic temperatures using compact devices.[5]

Photon pair sources in competing platforms, such as lithium niobate on insulator (LNOI), have been demonstrated to have even higher chip generation rates by utilizing the more efficient SPDC process. Ma *et al.* have reported a periodically polled ring resonator with generation rates of 2.7 MHz/μW and a CAR exceeding 100.[15] LNOI micro-disk resonators have also been demonstrated with a generation rate of 5.13 MHz/μW and a CAR of 804.[16] While LNOI

also has an electro-optic response, its largest Pockels tensor element is r_{42} = 32.6 pm/V, while BTO possesses r_{42} = 1640 pm/V.[17]

In this article, we show that as part of a $\chi^{(3)}$ photon pair source, the presence of a BTO layer does not appear to hinder the photon pair generation rate when comparing to brightness values from similar devices in silicon-on-insulator (SOI). We use the effective non-linearity from SFWM, γ_{eff} to quantify this.

II. METHODS

We tested the platform by characterizing a series of ring resonator devices with a 2.5 mm bus waveguide section. To compare to the brightness values of waveguide and ring resonator devices in the literature, we measured the device both on- and off-resonance. This was done by controlling the temperature to isolate the contribution from the bus waveguide section and filter the signal and idler wavelengths each with a bandwidth of 0.5 nm and separated 4.8 nm from the pump filter.

The setup shown in Fig. 1 was employed to characterize the photon generation process in this hybrid platform. A pulsed laser centered at 1550.97 nm with the bandwidth of 0.52 nm and the pulse width of 1 ps was amplified with an erbium-doped fiber amplifier (EDFA) to generate the strong pump for this process. Then, this was passed through a variable optical attenuator (VOA) to allow full tunability of the power down to −60 dB without changing the pulse properties. Two dense wavelength-division multiplexer (DWDM) filters ≥80 dB of combined rejection band suppression were used to eliminate pump noise from the noise floor of the laser entering the signal and idler collection bandwidths. These were placed before a polarization controller to allow optimization of the inserted light for TE polarization that the grating couplers were designed for. A 99:1 beam splitter allowed monitoring of the power coupled to the device under test (DUT) through a V-groove optical fiber array mounted to one arm of the probe station. After the output from the probe station, a multi-channel DWDM module was used

to de-multiplex the signal and idler frequencies and reject the pump. Then, an extra single-channel DWDM was placed on the signal and idler channels for additional filtering. This filtering after the chip also offered ≥80 dB of rejection band suppression for each channel. Finally, the two channels were routed through a fiber network to two PhotonSpot superconducting nano-wire single photon detectors (SNSPDs) connected to a time interval analyzer (TIA).

The coupling was optimized in both position and polarization before each measurement with the pulsed laser and the total coupling loss from the pair of input and output grating couplers, $\eta_{coupling}$ measured. The chip was mounted to the sample stage of a LakeShore CPX probe station using thermal resin, and the temperature of this stage was controlled using a resistive heater controlled by a temperature controller. The VOA was set to sweep over a set of attenuation values to yield the characteristic plots shown in Fig. 2. It was also necessary to limit the total time taken to carry out the measurements to limit the effect of the coupling drift. The integration time was varied between 30 and 300 seconds, depending on the level of attenuation. This was to ensure that the number of coincidence and single counts remained roughly constant and to minimize the statistical variation across the measurements.

To find γ_{eff} for SFWM, a set of three quadratic equations can be used to model and fit a set of data, which is taken by measuring the signal count rate, idler count rate, and the signal–idler coincidence count rate as a function of power.[18] For our devices, we found that a non-negligible imbalance of the input and output grating coupler efficiencies leads to an over or under estimation of γ_{eff} when calculated in this way. This depends on which grating coupler is chosen to be the input or output and increases the uncertainty in γ_{eff}. We propose a method outlined in the supplementary material that was inspired by the work of Sinclair et al.[19] This reduces the overall uncertainty and was used to calculate the γ_{eff} for our devices.

The integration of counts for each attenuation value set on the VOA was repeated 10 times for each configuration, and the standard error calculated from these repeated measurements were passed as

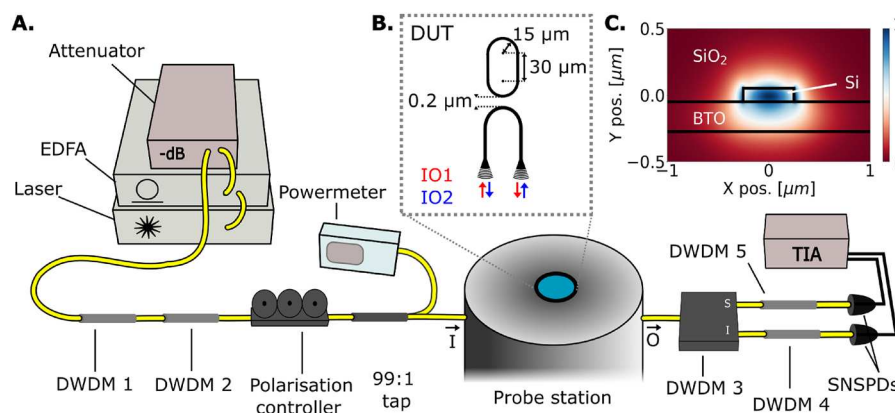**FIG. 1.** (a) Experimental setup used for characterizing the device under test (DUT). (b) Schematic of a DUT with a coupling gap of 0.2 μm and bus waveguide length of 2.5 mm. The two possible grating coupler input and output configurations are labeled IO1 and IO2. (c) Electric field distribution of the fundamental TE mode in a waveguide cross section of the DUT. The details of all equipment are tabulated in Table S2.
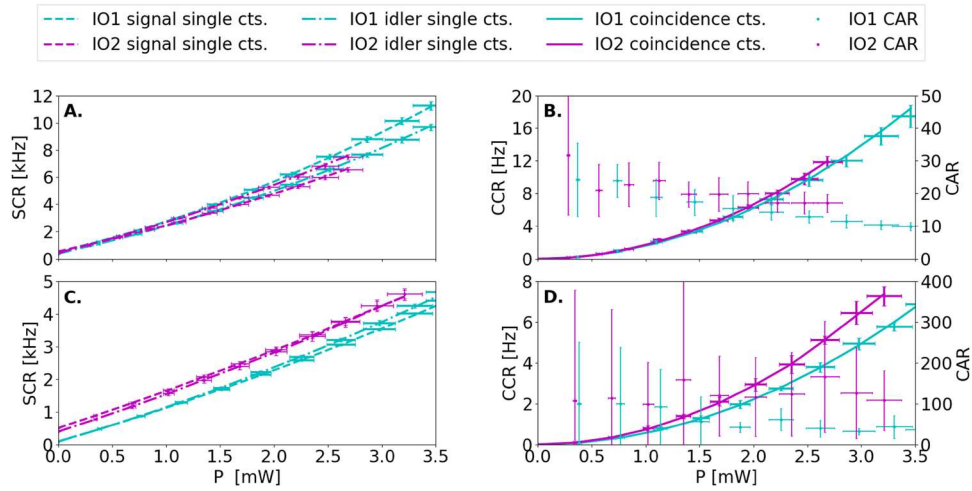
FIG. 2. Raw single count rates (SCRs) as a function of pump power are shown for (a) on-resonance and (c) off-resonance. Coincidence count rates (CCRs) and CAR as a function of pump power are shown on the right panes for (b) on-resonance and (d) off-resonance. The cyan and magenta lines represent the IO1 and IO2 configurations, respectively. The dashed, dashed–dotted, and solid lines represent the signal, idler, and coincidence count rates respectively. Raw count rates are represented by the bold error bars, and the CAR values are represented by the light error bars.

TABLE I. Comparison of the reported photon pair source brightness measurements in order of magnitude of γ_{eff} reported. *In cases where a γ_{eff} value was not directly reported, this was extrapolated using the maximum coincidence count rate and corresponding value for power. The geometry is defined as material (waveguide width × waveguide height) for strip waveguide geometry with/material (slab thickness) added for rib waveguide geometry. The excitation methods used were a continuous wave (CW) or pulsed laser pump with one scheme using additional reverse biasing (RB). Q is defined as the loaded quality factor.

(a) Comparison of waveguide sources

Refs.	Geometry (nm)	Excitation	CAR	L (mm)	γ_{ef} (MHz/mW^2)
20	SiN(550 × 300)	CW	7	10	0.009
21	Si(500 × 220)	Pulsed	14	· · ·	1.1
22	AlGaAs(700 × 600)	Pulsed	177	4.5	1.91
This work	Si(500 × 100)/BTO(225)	Pulsed	108	2.5	2.0 ± 0.3
23	Si(100 × 220)	Pulsed	25	9.11	2.5

(b) Comparison of ring resonator sources

Refs.	Geometry (nm)	Excitation	CAR	C (µm)	Q (×10^4)	γ_{eff} (MHz/mW^2)
24	SiN(8000 × 950)	CW	1864 ± 571	386.4	100	1.03 ± 0.09
25	Si(500 × 220)	CW	30	42.7	1	1.9
26	Si(500 × 220)	Pulsed; RB	602 ± 37	62.8	4	5.3
27	Si(400 × 220)	CW	>350	62.8	10	5.8
28	Si(500 × 220)	Pulsed	>100	· · ·	5	6.1
29	Si(650 × 220)/Si[70]	Pulsed	3000 ± 500	62.8	9	14.6
This work	Si(500 × 100)/BTO(225)	Pulsed	32 ± 19	248.2	7	14.7 ± 1.3
30	Si(500 × 220)	Pulsed	· · ·	111.8	6	19.9
31	Si(500 × 220)	Pulsed	10	94.2	· · ·	30.6
32	Si(650 × 220)/Si(70)	CW; RB	12 105 ± 1821	62.8	9	146 ± 6

a parameter in a least-squares fit. The errors in the quadratic coefficients were then obtained from the covariance matrix of these fits.

III. RESULTS AND DISCUSSION

Table I presents that the value we report for γ_{eff} compares favorably with other waveguide and microring resonator sources where a similar method of excitation is used. We note that a large linear component to the signal and idler count rates is certainly a source of uncertainty in our values. Despite the filtering used having ≥80 dB of rejection band suppression on each channel, this still resulted in a small (of the order of 10^2 Hz) amount of pump leakage. Suppressing this further would require longer integration times to detect a sufficient number of coincidence events, which is already low due to high losses inherent in the system. In addition, $\eta_{coupling}$ was measured to be ~20 dB. The high insertion loss has been shown not to be due to the BTO layer.[6] It is likely due to a combination of the use of non-optimized grating couplers and a lack of pitch control on the optical arm of the probe station. The loss of the optical connection from where the probe station is located to the detector system was measured to be ~4 dB for each channel. Longer integration times also risk coupling drift over the series of measurements, which arise due to thermal fluctuations in the environment.

Our reported value for the coincidence-to-accidental ratio (CAR, the details outlining our calculation of this is provided in the supplementary material) is relatively low compared to other values presented in Table I. The main factor contributing to this is the high channel loss as this increases the probability of broken pairs contributing to the accidental counts. The large error in the CAR is due to the very small number of accidental counts observed at the lowest pump power. This was particularly apparent in the off-resonance case. A higher value with lower uncertainty could be achieved if coupling could be sustained at lower pump powers for a longer integration time of the order of several hours. The lowest pump power setting used was 0.3 mW with an integration time of 300 s. Ma *et al.*[29] achieve a CAR of 2873 using a comparable amount of pulsed pump power in the waveguide but a longer integration time of 3000 seconds. They also report a ~7 dB better collection efficiency of photons generated in the waveguide, which is likely a factor in this higher value.

We have demonstrated photon generation via SFWM in these devices at room temperature. Given the results of recent studies on Si[33] and the cryogenic compatibility of the electro-optic effect in these devices,[6] we expect a good photon generation performance at cryogenic temperatures as well.

Here, we have shown that the effective non-linearity of a hybrid Si–BTO integrated photon pair source is comparable to an all-Si one and appears to provide an enhancement compared to some reported values.[21,25–29] Together with the work of Eltes *et al.*,[5] our results support the case for implementing this platform in scenarios where high speed modulation and high brightness photon pair generation are required.

IV. CONCLUSIONS

In this article, we demonstrate that a hybrid Si–BTO platform shows a similar or better performance than an SOI platform in terms of SFWM brightness. We characterize the brightness of our source by analyzing coincidence and single count rates as a function of the injected pump power, which leads to a calculated γ_{eff} of (14.7 ± 1.3) and (2.0 ± 0.3) MHz/mW^2 for the on- and off-resonance conditions, respectively. Given that these devices were not optimized for photon generation, higher brightness could likely be achieved by fine-tuning the dispersion engineering of the waveguide geometry. The maximum CAR value between 32 ± 19 and 24 ± 12 is reasonable compared to other values quoted in the literature. However, a higher value with lower uncertainty could be achieved with more efficient coupling structures and lower loss detection channels. Future studies repeating this experiment at low temperatures could demonstrate the predicted cryogenic compatibility of these devices and the effect on source brightness. In summary, we conclude that the presence of a BTO layer in a hybrid Si–BTO device provides no drawbacks in terms of brightness of the photon pair source while providing EOM capabilities.

SUPPLEMENTARY MATERIAL

The supplementary material contains details of the equipment shown in Fig. 1 and spectral data of the DUT in the on- and off-resonance configurations. Specific details on how the CAR was calculated and a derivation of the method used to calculate the effective non-linearity are also included.

AUTHOR DECLARATIONS

Conflict of Interest

The authors have no conflicts to disclose.

Author Contributions

D. Marchant: Data curation (equal); Formal analysis (equal); Investigation (equal); Methodology (equal); Writing – original draft (equal); Writing – review & editing (equal). **I. Faruque**: Supervision (equal); Validation (equal); Writing – review & editing (equal). **J. Barreto**: Conceptualization (equal); Funding acquisition (equal); Methodology (equal); Project administration (equal); Supervision (equal); Writing – review & editing (equal).

DATA AVAILABILITY

The data that support the findings of this study are available within the article and its supplementary material.

REFERENCES

[1] E. Knill, R. Laflamme, and G. J. Milburn, "A scheme for efficient quantum computation with linear optics," Nature **409**, 46–52 (2001).

[2] P. Kok, W. J. Munro, K. Nemoto, T. C. Ralph, J. P. Dowling, and G. J. Milburn, "Linear optical quantum computing with photonic qubits," Rev. Mod. Phys. **79**, 135–174 (2007).

[3] N. Gisin and R. Thew, "Quantum communication," Nat. Photonics **1**, 165–171 (2007).

[4] X. Ma and H.-K. Lo, "Quantum key distribution with triggering parametric down-conversion sources," New J. Phys. **10**, 073018 (2008).

[5] F. Eltes, C. Mai, D. Caimi, M. Kroh, Y. Popoff, G. Winzer, D. Petousi, S. Lischke, J. E. Ortmann, L. Czornomaz, L. Zimmermann, J. Fompeyrine, and S. Abel, "A BaTio₃-based electro-optic pockels modulator monolithically integrated on an advanced silicon photonics platform," J. Lightwave Technol. **37**, 1456–1462 (2019).

[6] F. Eltes, G. E. Villarreal-Garcia, D. Caimi, H. Siegwart, A. A. Gentile, A. Hart, P. Stark, G. D. Marshall, M. G. Thompson, J. Barreto, J. Fompeyrine, and S. Abel, "An integrated optical modulator operating at cryogenic temperatures," Nat. Mater. **19**, 1164–1168 (2020).

[7] F. Eltes, M. Kroh, D. Caimi, C. Mai, Y. Popoff, G. Winzer, D. Petousi, S. Lischke, J. E. Ortmann, L. Czornomaz, L. Zimmermann, J. Fompeyrine, and S. Abel, "A novel 25 Gbps electro-optic pockels modulator integrated on an advanced si photonic platform," in *2017 IEEE International Electron Devices Meeting (IEDM)* (IEEE, 2017), pp. 24.5.1–24.5.4.

[8] F. Eltes, D. Caimi, F. Fallegger, M. Sousa, E. O'Connor, M. D. Rossell, B. Offrein, J. Fompeyrine, and S. Abel, "Low-loss BaTio₃–Si waveguides for nonlinear integrated photonics," ACS Photonics **3**, 1698–1703 (2016).

[9] L. Caspani, C. Xiong, B. J. Eggleton, D. Bajoni, M. Liscidini, M. Galli, R. Morandotti, and D. J. Moss, "Integrated sources of photon quantum states based on nonlinear optics," Light Sci. Appl. **6**, e17100 (2017).

[10] R. Boyd, *Chapter 1. The Nonlinear Optical Susceptibility* (Academic Press, 2003), pp. 1–65.

[11] G. Cocorullo, F. G. Della Corte, I. Rendina, and P. M. Sarro, "Thermo-optic effect exploitation in silicon microstructures," Sens. Actuators, A **71**, 19–26 (1998).

[12] R. Soref and B. Bennett, "Electrooptical effects in silicon," IEEE J. Quantum Electron. **23**, 123–129 (1987).

[13] U. Chakraborty, J. Carolan, G. Clark, D. Bunandar, G. Gilbert, J. Notaros, M. R. Watts, and D. R. Englund, "Cryogenic operation of silicon photonic modulators based on the DC Kerr effect," Optica **7**, 1385–1390 (2020).

[14] J. Komma, C. Schwarz, G. Hofmann, D. Heinert, and R. Nawrodt, "Thermo-optic coefficient of silicon at 1550nm and cryogenic temperatures," Appl. Phys. Lett. **101**, 041905 (2012).

[15] Z. Ma, J.-Y. Chen, Z. Li, C. Tang, Y. M. Sua, H. Fan, and Y.-P. Huang, "Ultrabright quantum photon sources on chip," Phys. Rev. Lett. **125**, 263602 (2020).

[16] B.-Y. Xu, L.-K. Chen, J.-T. Lin, L.-T. Feng, R. Niu, Z.-Y. Zhou, R.-H. Gao, C.-H. Dong, G.-C. Guo, Q.-H. Gong *et al.*, "Spectrally multiplexed and bright entangled photon pairs in a lithium niobate microresonator," Sci. China: Phys., Mech. Astron. **65**, 294262 (2022).

[17] R. W. Boyd, *Chapter 11–The Electooptic and Photorefractive Effects*, in *Nonlinear Optics*, 4th ed., edited by R. W. Boyd (Academic Press, 2020), pp. 495–522.

[18] D. Bonneau, J. W. Silverstone, and M. G. Thompson, *Silicon Photonics III: Systems and Applications* (Springer, 2016), pp. 41–82.

[19] G. F. Sinclair, N. A. Tyler, D. Sahin, J. Barreto, and M. G. Thompson, "Temperature dependence of the kerr nonlinearity and two-photon absorption in a silicon waveguide at 1.55 μm," Phys. Rev. Appl. **11**, 044084 (2019).

[20] J. W. Choi, B.-U. Sohn, G. Chen, D. Ng, and D. Tan, "Correlated photon pair generation in ultra-silicon-rich nitride waveguide," Opt. Commun. **463**, 125351 (2020).

[21] I. I. Faruque, G. F. Sinclair, D. Bonneau, T. Ono, C. Silberhorn, M. G. Thompson, and J. G. Rarity, "Estimating the indistinguishability of heralded single photons using second-order correlation," Phys. Rev. Appl. **12**, 054029 (2019).

[22] P. Kultavewuti, E. Y. Zhu, L. Qian, V. Pusino, M. Sorel, and J. Stewart Aitchison, "Correlated photon pair generation in AlGaAs nanowaveguides via spontaneous four-wave mixing," Opt. Express **24**, 3365–3376 (2016).

[23] J. E. Sharping, K. F. Lee, M. A. Foster, A. C. Turner, B. S. Schmidt, M. Lipson, A. L. Gaeta, and P. Kumar, "Generation of correlated photons in nanoscale silicon waveguides," Opt. Express **14**, 12388–12393 (2006).

[24] K. Wu, Q. Zhang, and A. W. Poon, "Integrated Si₃N₄ microresonator-based quantum light sources with high brightness using a subtractive wafer-scale platform," Opt. Express **29**, 24750–24764 (2021).

[25] S. Clemmen, K. P. Huy, W. Bogaerts, R. G. Baets, P. Emplit, and S. Massar, "Continuous wave photon pair generation in silicon-on-insulator waveguides and ring resonators," Opt. Express **17**, 16558–16570 (2009).

[26] E. Engin, D. Bonneau, C. M. Natarajan, A. S. Clark, M. G. Tanner, R. H. Hadfield, S. N. Dorenbos, V. Zwiller, K. Ohira, N. Suzuki, H. Yoshida, N. Iizuka, M. Ezaki, J. L. O'Brien, and M. G. Thompson, "Photon pair generation in a silicon micro-ring resonator with reverse bias enhancement," Opt. Express **21**, 27826–27834 (2013).

[27] M. Fujiwara, R. Wakabayashi, M. Sasaki, and M. Takeoka, "Wavelength division multiplexed and double-port pumped time-bin entangled photon pair generation using Si ring resonator," Opt. Express **25**, 3445–3453 (2017).

[28] I. I. Faruque, G. F. Sinclair, D. Bonneau, J. G. Rarity, and M. G. Thompson, "On-chip quantum interference with heralded photons from two independent micro-ring resonator sources in silicon photonics," Opt. Express **26**, 20379–20395 (2018).

[29] C. Ma, X. Wang, and S. Mookherjea, "Photon-pair and heralded single photon generation initiated by a fraction of a 10 Gbps data stream," Opt. Express **26**, 22904–22915 (2018).

[30] Q. Zheng, J. Liu, C. Wu, S. Xue, P. Zhu, Y. Wang, X. Yu, M. Yu, M. Deng, J. Wu, and P. Xu, "Bright 547-dimensional Hilbert-space entangled resource in 28-pair modes biphoton frequency comb from a reconfigurable silicon microring resonator," Chin. Phys. B **31**, 024206 (2022).

[31] J. W. Silverstone, R. Santagati, D. Bonneau, M. J. Strain, M. Sorel, J. L. O'Brien, and M. G. Thompson, "Qubit entanglement between ring-resonator photon-pair sources on a silicon chip," Nat. Commun. **6**, 7948 (2015).

[32] C. Ma, X. Wang, V. Anant, A. D. Beyer, M. D. Shaw, and S. Mookherjea, "Silicon photonic entangled photon-pair and heralded single photon generation with car > 12,000 and $g^{(2)}(0) < 0.006$," Opt. Express **25**, 32995–33006 (2017).

[33] L.-T. Feng, Y.-J. Cheng, X.-Z. Qi, Z.-Y. Zhou, M. Zhang, D.-X. Dai, G.-C. Guo, and X.-F. Ren, "Entanglement generation using cryogenic integrated four-wave mixing," Optica **10**, 702–707 (2023).